hcp-bcc structural phase transformation of titanium: Analytic model calculations

K. Masuda-Jindo
Department of Materials Science and Engineering, Tokyo Institute of Technology, Nagatsuta, Midori-ku, Yokohama 226-8503, Japan

S. R. Nishitani
Department of Materials Science and Engineering, Kyoto University, Sakyo-ku, Kyoto, 606-8501, Japan

Vu Van Hung
Hanoi National Pedagogic University, km8 Hanoi-Sontay Highway, Hanoi, Vietnam

(Received 29 July 2003; revised manuscript received 26 August 2004; published 23 November 2004)

We show that the hcp (α)→bcc (β) structural phase transformation of titanium occurs via anharmonicity effect of thermal lattice vibrations. The full-potential linear muffin-tin orbital method in the local density approximation with the generalized gradient correction is used to derive the embedded atom potential for Ti, which allows us the analytic and realistic calculations of the thermodynamic quantities. We also discuss the similar phase transformation but slightly different mechanism occurring in zirconium in terms of the anharmonicity of thermal lattice vibrations.

DOI: 10.1103/PhysRevB.70.184122 PACS number(s): 65.40.−b, 71.15.−m

I. INTRODUCTION

Since the pioneering work by Zener,[1] there have been extensive experimental and theoretical works[2–18] on the phase transformations of metals and alloys. The important and fascinating elements of the structural phase transformations are hcp transition metals (IV-B group of elements) Ti, Zr, and Hf, which exhibit hcp (α-phase)→bcc (β-phase) structural transitions at temperatures 1155, 1135, and 2015 K, respectively. These elements are also interesting due to the appearance of omega (ω) phases at high pressures as well as in conjunction with the martensitic phase transitions.[5] However, there have been crucial lattice dynamical problems for early transition-metal elements (Sc, Ti, Y, Zr, La, and Hf) that certain phonon branches are unstable. The first-principles calculations of the phonon dispersion have shown that the entire transverse $[\xi\ \xi\ 0]$ branch with polarization along $[\bar{1}10]$ and the longitudinal $\mathbf{L}[\frac{2}{3}\frac{2}{3}\frac{2}{3}]$ phonon are unstable in the harmonic approximation.[6,9] Therefore, it has been believed that they are stabilized by the anharmonic effects at high temperatures, but it has never been shown that the free energies of bcc phases are actually lower than those of hcp phases in the high-temperature region, including the anharmonicity contributions.

In the present article, the Helmholtz free energies of crystalline systems are derived in analytic forms using the moment expansion technique in the quantum statistical mechanics,[20,21] hereafter referred to as the statistical moment method (SMM). We will show that the hcp→bcc structural phase transition of Ti occurs via anharmonicity effects of thermal lattice vibrations: The anharmonicity contributions of thermal lattice vibrations are much larger (for bcc phase of Ti crystal) than those of the electronic entropies.[12,13] We note that it has been a longstanding and puzzling problem to draw definite conclusion on the role of the vibrational entropies on the hcp→bcc structural phase transitions of IV-B elements, especially for titanium. We will calculate the temperature dependence of free energies of Ti crystals, in comparison with those of Zr crystals.

The format of the present paper is as follows: In Sec. II, the general derivations by the statistical moment method are given for the thermodynamic quantities of the hcp metals. The calculation results of hcp→bcc transitions of Ti and Zr are presented in Secs. III A and III B, respectively. The mechanical instabilities of bcc phases at low temperatures are discussed in Sec. III B. The final Sec. IV is devoted to the conclusions.

II. THEORY

Let us consider a quantum system written by the following Hamiltonian:

$$\hat{H} = \hat{H}_0 - \sum_i \alpha_i \hat{V}_i, \tag{1}$$

where $\hat{H}_0$ denotes the lattice Hamiltonian in the harmonic approximation, and the second term is due to the anhamonicity of thermal lattice vibrations. α_i denotes a parameter characterizing the anharmonicity of lattice vibrations and $\hat{V}_i$ the related operator. The Helmholtz free energy of the system given by Hamiltonian (1) is formally given by

$$\Psi = \Psi_0 - \sum_i \int_0^{\alpha_i} \langle \hat{V}_i \rangle_a d\alpha_i, \tag{2a}$$

$$\langle \hat{V}_i \rangle_a = -\partial \Psi / \partial \alpha_i, \tag{2b}$$

where $\langle \cdots \rangle_a$ expresses the expectation values at the thermal equilibrium with the (anharmonic) Hamiltonian $\hat{H}$. Ψ denotes the free energy of the system at temperature T, and Ψ_0 is the free energy of the harmonic lattice corresponding to the Hamiltonian $\hat{H}_0$. The expectation values in the above Eq.

(2) are evaluated with the use of the density matrix formalism

$$\langle \hat{V} \rangle_a = \mathrm{Tr}[\hat{\rho}\hat{V}], \tag{3}$$

where the density matrix $\hat{\rho}$ is defined, with $\theta = k_B T$, as

$$\hat{\rho} = \exp\left[\frac{\Psi - \hat{H}}{\theta}\right]. \tag{4}$$

Firstly, we expand the potential energy of the system in terms of the thermal atomic displacements

$$U = \sum_i \left\{ E_i^0 + \sum_{\alpha,\beta} \left(\frac{\partial^2 E_i}{\partial u_{i\alpha}\partial u_{i\beta}}\right)_{eq} u_{i\alpha}u_{i\beta} + \frac{1}{3}\sum_{\alpha,\beta,\gamma}\left(\frac{\partial^3 E_i}{\partial u_{i\alpha}\partial u_{i\beta}\partial u_{i\gamma}}\right)_{eq} u_{i\alpha}u_{i\beta}u_{i\gamma} + \frac{1}{12}\sum_{\alpha,\beta,\gamma,\eta}\left(\frac{\partial^4 E_i}{\partial u_{i\alpha}\partial u_{i\beta}\partial u_{i\gamma}\partial u_{i\eta}}\right)_{eq} u_{i\alpha}u_{i\beta}u_{i\gamma}u_{i\eta} + \cdots \right\}, \tag{5}$$

where $u_{i\alpha}$ denotes α-Cartesian component of the atomic displacement of ith atom. Using Eq. (5), the thermal average of potential energy of the hcp crystal is given in terms of the power moments $\langle u^n \rangle$ of the thermal atomic displacements and harmonic parameter k, and three anharmonic expansion coefficients β, γ_1, and γ_2 as

$$\langle U \rangle = U_0 + 3N\left(\frac{k}{2}\langle u^2\rangle + \beta\langle u\rangle\langle u^2\rangle + \gamma_1\langle u^4\rangle + \gamma_2\langle u^2\rangle^2 + \cdots\right), \tag{6}$$

where

$$k = \left(\frac{\partial^2 E_i}{\partial u_{i\alpha}^2}\right)_{eq}, \quad \beta = \left(\frac{\partial^3 E_i}{\partial u_{i\alpha}\partial u_{i\beta}^2}\right)_{eq},$$

$$\gamma_1 = \frac{1}{24}\left(\frac{\partial^4 E_i}{\partial u_{i\alpha}^4}\right)_{eq}, \quad \gamma_2 = \frac{6}{24}\left(\frac{\partial^4 E_i}{\partial u_{i\alpha}^2 u_{i\beta}^2}\right)_{eq}, \tag{7}$$

with $\alpha \neq \beta = x$, y, or z. In the above Eq. (7), eq means the thermal averaging over the equilibrium ensemble. Here, we note that the above treatment of the moment expansion technique has been done in a similar fashion to the so-called "potential switch" Monte Carlo (MC) method.[22] In this method for treating solid phase, the "Einstein crystal" is taken as reference system, for which the exact free energy expressions are well known. The physical quantities are derived from the thermal averages of sufficiently large numbers of random configurations. The similarity between the present SMM and potential switch MC method are discussed in more details in the Appendix. By using our "real space" approach, we bypass the anomalous phonon branches in the phonon dispersions in deriving the thermodynamic quantities.

Using moment expansion formulas,[20,21] one can find the lowest-order moments $\langle u^2 \rangle$ and $\langle u^4 \rangle$ of the hcp crystal as

$$\langle u^2 \rangle = \frac{\theta}{K} x \coth x + \frac{2}{3}\frac{2\gamma\theta^2}{K^3}a_1 + \frac{2\gamma^2\theta^3}{K^5}a_1(2a_1 - 1), \tag{8}$$

$$\langle u^4 \rangle = -\frac{8\theta^2}{3K^2}\left(\frac{a_1}{4} + \frac{\gamma^2\theta^2}{K^4}a_2\right) - \frac{2\gamma\theta^3}{K^4}a_1(2a_1 - 1) - \frac{2\gamma^2\theta^4}{K^6}a_1\left[\frac{2a_1}{3} - (2a_1 - 1)(2a_1 + 3)\right], \tag{9}$$

where

$$a_1 = 1 + x \coth x/2, \tag{10a}$$

$$a_2 = 13/3 + 47x \coth x/6 + 23x^2 \coth x^2/6 + x^3 \coth x^3/2, \tag{10b}$$

$$x = \hbar\omega/2\theta \equiv \hbar\sqrt{k/m}/2\theta, \tag{10c}$$

$$\gamma = 4(\gamma_1 + \gamma_2), \tag{10d}$$

$$K = k - \beta^2/3\gamma. \tag{10e}$$

The Helmholtz free energy Ψ of our system (hcp α-phase) can be derived from the functional form of the internal energy of the above Eq. (6) through the straightforward analytic integrations I_1, I_2, and I_3, with respect to the three anharmonicity "variables" γ_2, γ_1, and β (fourth-order moment approximation):

$$I_1 = \int_0^{\gamma_2} \langle u^2\rangle^2 \Big|_{\substack{\gamma_1=0 \\ \beta=0}} d\gamma_2, \; I_2 = \int_0^{\gamma_1} \langle u^4\rangle\big|_{\beta=0} d\gamma_1,$$

$I_3 = \int_0^{\beta} \langle u\rangle\langle u^2\rangle d\beta$. The final expression of the Helmholtz free energy is given by

$$\Psi = u_0 + 3N\theta[x + \ln(1 - e^{-2x})] + 3N\left\{\frac{\theta^2}{K^2}\left[\gamma_2 x^2 \coth^2 x - \frac{2\gamma_1}{3}a_1\right] + \frac{2\theta^3}{K^4}\left[\frac{4}{3}\gamma_2^2 a_1 x \coth x - 2(\gamma_1^2 + 2\gamma_1\gamma_2)a_1(2a_1 - 1)\right] + \left(\frac{2\gamma a_1}{3K^3}\right)^{1/2}\frac{\beta}{K}\theta^2 + \left[\left(\frac{2\gamma a_1}{3K^3}\right)^{3/2}\beta + \frac{2k\gamma}{K^6}\beta^2\right]\theta^3\right\}. \tag{11}$$

Similar expressions of the Helmholtz energy can be also given for cubic crystals.[21] The Helmholtz energies Ψ are then used to calculate the various thermodynamic quantities and to investigate the hcp$\rightarrow$bcc phase transitions of IV-B elements. Here, we note that we do not use the phonon dispersion curves calculated in the harmonic approximation (the anharmonicity of the thermal lattice vibrations is taken into account as a correction term) which causes the difficulties in calculating the free energy of the bcc phase of early transition-metal elements[6,19] at low temperatures. The various thermodynamic quantities, such as specific heats, thermal lattice expansion coefficients, elastic moduli, and Grüneisen constant, which are closely related to the

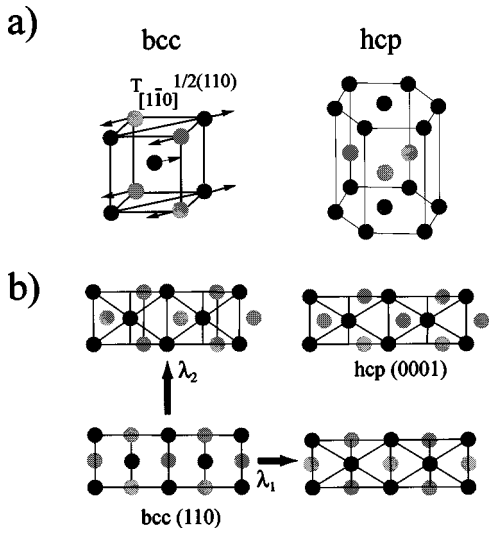

FIG. 1. Schematic representation of the bcc→hcp transition, with λ_1 and λ_2 distortion modes.

anharmonicity of thermal lattice vibrations, are derived from the Helmholtz free energy Ψ of Eq. (11).

The specific heats C_V and C_P at constant volume and constant pressure, respectively, are given by

$$C_V = 3Nk_B\left\{\frac{x^2}{\sin h^2 x} + \frac{2\theta}{K^2}\left[\left(2\gamma_2 + \frac{\gamma_1}{3}\right)\frac{x^3\coth x}{\sin h^2 x} + \frac{\gamma_1}{3}\left(1 + \frac{x^2}{\sin h^2 x}\right) - \gamma_2\left(\frac{x^4}{\sin h^4 x} + 2\frac{x^4\coth^2 x}{\sin h^2 x}\right)\right] - 2\left(\frac{2}{3}\frac{\gamma a_1}{K^3}\right)^{1/2}\frac{\beta}{K}\theta - 6\left[\left(\frac{2}{3}\frac{\gamma a_1}{K^3}\right)^{3/2}\beta + \frac{2k\gamma^2}{K^6}\beta^2\right]\theta^2\right\} \tag{12a}$$

and

$$C_P = C_V + \frac{9TV\alpha^2}{\chi_T}. \tag{12b}$$

The isothermal and adiabatic compressibilities (inverse of the bulk moduli) are derived from the free energy of Eq. (11) as

$$\chi_T = -\frac{1}{V_0}\left(\frac{\partial V}{\partial P}\right)_T = 2\left(\frac{a}{a_0}\right)^2\left(\frac{c}{c_0}\right)\Bigg/\left[P + \frac{2\sqrt{3}}{c}\frac{1}{3N}\left(\frac{\partial^2\Psi}{\partial a^2}\right)_T\right], \tag{13a}$$

$$\chi_s = \frac{C_V}{C_P\chi_T}, \tag{13b}$$

where P denotes the pressure, and (a,c) and (a_0,c_0) are the lattice spacings of hcp crystal at temperature T and those values at $T=0$, respectively. On the other hand, the Grüneisen constant γ_g can be derived straightforwardly from the volume dependence of the vibrational frequency ω.

III. RESULTS AND DISCUSSIONS

To describe the bcc to hcp transition, we consider Burger's distortions.[23] Keeping the atomic volume at a constant, the simplest paths of transition from a bcc lattice into the hcp structure are through the base-centered orthorhombic (oS4 in Pearson's symbol; space group Cmcm) structure, as schematically shown in Fig. 1. This includes a shear deformation from bcc (110) plane to the hexagonal basal plane and an alternate slide along $[1\bar{1}0]$ of the planes (T_1N mode in bcc).

Intermediate oS4 structures are mapped on a two-dimensional parameter space in terms of λ_1 and λ_2: We take λ_1 to represent the shear deformation and λ_2 the slide displacement. The bcc and hcp structures are denoted by (0,0) and (1,1), respectively. Taking bcc lattice constant a, the orthorhombic lattice parameters are written as

$$a_0(\lambda_1) = a/\alpha(\lambda_1),$$

$$b_0(\lambda_1) = \alpha(\lambda_1)\sqrt{2}a,$$

$$c_0 = \sqrt{2}a,$$

where

$$\alpha(\lambda_1) = 1 + \{(3/2)^{(1/4)} - 1\}\lambda_1.$$

Here, a is the lattice constant and α is the parameter: $\alpha=0$ for bcc and $\alpha=1$ for hcp structures.

Furthermore, the primitive cell has one of the atoms at

$$\overline{\tau}(\lambda_1+\lambda_2) = \left[0, \frac{3+\lambda_2}{12}b_0(\lambda_1), \frac{1}{4}c_0\right].$$

The detailed features in the energy surfaces, so-called Burger's surfaces (which will be presented in Fig. 2 for Ti crystal), for the bcc→hcp phase transitions are of great importance in analyzing the phase transitions of titanium group of elements.

A. Titanium crystal

In order to reduce the numerical inaccuracies in the calculation of the free energies of the metallic systems, we employ the analytic form of embedded atom method (EAM) type of potentials. In particular, the full-potential linear muffin-tin orbital method (FP-LMTO)[24,25] is used to derive the EAM potential for Ti crystal. In the FP-LMTO, the core energy shifts and Perdew and Wang type of generalized-gradient approximation (GGA)[26] are included. In the calculations, particular attention has also been paid to the total energy convergence because of small energy differences between bcc and hcp structures. Very stable convergence is attained by evaluating the total energy using the Harris-Foulkes[27,28] energy functional of the output and input electron densities at each iteration.[25] The ground state total energies of bcc, hcp, and ω phases of Ti crystal are calculated to be −0.477 43, −0.484 29, and −0.484 24 Ry/atom, respectively. The bulk moduli of bcc, hcp, and ω phases of Ti crystals are 107, 112, and 112 GPa, respectively. The shear elastic constant C' of bcc phase is negative and −22.7 GPa.

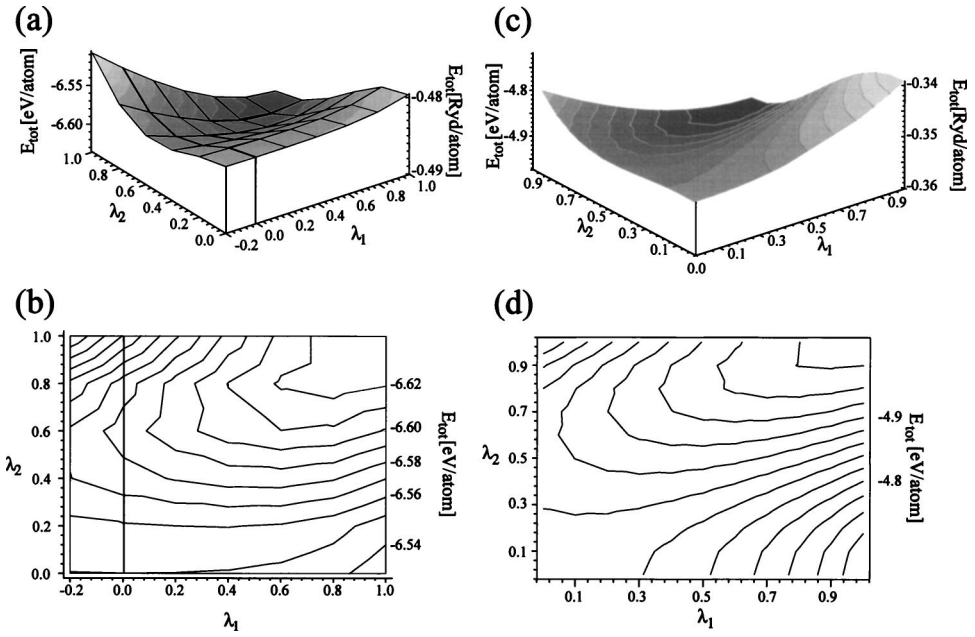

FIG. 2. Adiabatic potential surface for Burger's path with contours of step 20 meV (1.47 mRy): (a) and (b) are from FP-LMTO method with GGA corrections, while (c) and (d) by the EAM potential of Eq. (14).

(All the elastic moduli are calculated without including the contributions of zero-point vibrations.) The calculated equilibrium atomic volume Ω of hcp crystal is $0.99\Omega_0$, Ω_0 being the experimental value. Thus, the present FP-LMTO method provides us the quite accurate cohesive energies, elastic moduli, and Burger's surfaces of Ti crystal from bcc to hcp structures.

The EAM potentials are composed of two terms, embedding function and interaction φ terms: $E=\varphi+\sqrt{\Sigma h^2(r)}$. To guarantee the transferability of EAM potentials for bcc and hcp phases, the spatial dependences of the above two terms are taken as

$$\varphi(r) = A \exp\left[-p\left(\frac{r}{r_0}-1\right)\right]\exp\left\{p\left[-\left(\frac{r}{r_c}\right)^{n_c}+\left(\frac{r_0}{r_c}\right)^{n_c}\right]\right\}, \tag{14a}$$

$$h(r) = B \exp\left[-q\left(\frac{r}{r_0}-1\right)\right]\exp\left\{q\left[-\left(\frac{r}{r_c}\right)^{n_c}+\left(\frac{r_0}{r_c}\right)^{n_c}\right]\right\}. \tag{14b}$$

The parameters of EAM potential of Ti crystal are chosen to be $q=2.8$, $p=12.6$, $r_c=1.4r_0$, $n_c=7.5$, $A=0.177\,621$ eV, and $B=-2.020\,161$ eV, so as to reproduce the overall features of the Burger's; surfaces calculated by FP-LMTO method, which are shown and compared in Fig. 2. In Fig. 2(a), we present the Burger's surfaces of Ti crystal calculated by FP-LMTO method, together with its projection onto the (λ_1 $-\lambda_2$) basal plane in Fig. 2(b). The corresponding results obtained by the EAM potential are shown in Figs. 2(c) and 2(d) respectively. The topological features of the Burger's surfaces of Figs. 2(c) and 2(d) by EAM potential are in good agreement with those of Figs. 2(a) and 2(b) by FP-LMTO method. One sees in Fig. 2 that there are considerable differences in the absolute values of Burger's surface energies between the two calculations. In the thermodynamic phase stability calculations, however, the relative stabilities between the hcp and bcc phases are of primary importance, and their absolute values are of less importance.

We have also checked the thermal expansion coefficients of Ti crystal calculated by the present SMM. From the definition of the linear thermal expansion coefficients α_T and the Helmholtz energy Ψ, α_T is simply given by $\alpha_T=(k_B\chi_T/3)\times(\partial P/\partial\theta)_V$, with $P=-(\partial\Psi/\partial V)_T$, where P is the pressure and χ_T the isothermal compressibility. The calculated linear thermal expansion coefficient α_T for α-phase of Ti crystal is $\alpha_T=9.8\times10^{-6}$ ($\deg^{-1}$) at room temperature, which compares favorably with the experimental results $8.2-10.4\times10^{-6}$ ($\deg^{-1}$).[29,30] The specific heats C_V and C_P given by Eqs. (12a) and (12b), respectively, are also strongly influenced by the anharmonicity of thermal lattice vibrations. In Table I, we present the calculated specific heats of α-Ti crystal as a function of the temperature, in comparison with the experimental results. In this calculation, the Lennard-Jones (L-J) type of potential (8.5–4.5 type one only fitting to experimental bulk modulus) is also used for comparison. One can see in Table I that the calculated temperature dependence of the specific heats of hcp Ti crystal are in good agreement with the experimental results. It is noticeable that the L-J type of potential gives also excellent results on the thermodynamic quantities of α-Ti crystal (although it underestimates the specific heats and it fails to predict the stability of bcc structure at the high temperature region). These results convince us to use the EAM potential for the energetics of hcp$\rightarrow$bcc phase transition of Ti crystal.

In Fig. 3 we show the temperature dependence of Helmholtz energies of Ti crystals for bcc, fcc, and hcp phases by dot-dashed, dashed, and solid curves, respectively. One sees in Fig. 3 that the Helmholtz energies of hcp and fcc phases are almost identical for temperature region lower than $\sim$500 K, and hcp phase becomes more stable than fcc phase for higher temperature than $\sim$500 K. The reason for the almost identical Helmholtz energies for lower temperatures is simply due to the fact that the EAM potential does not give

TABLE I. Calculated specific heats C_V and C_P of α-Ti.

Potential	T(K)	300	400	500	600	700	800	900
	a(Å)	2.9583	2.9622	2.9661	2.9698	2.9733	2.9768	2.9801
EAM	C_V (cal/mol K)	5.74	5.90	5.98	6.05	6.10	6.15	6.19
EAM	C_P (cal/mol K)	5.92	6.14	6.29	6.43	6.52	6.60	6.71
L-J	C_V (cal/mol K)	5.67	5.83	6.92	5.97	6.02	6.05	6.08
L-J	C_P (cal/mol K)	5.80	6.00	6.12	6.21	6.29	6.36	6.42
	$C_P^{\exp}$ (cal/mol K)	5.97	6.26	6.51	6.76	7.01	7.27	···

the differences in the ground state total energies between the hcp and fcc structures and the same mathematical form is used for the harmonic free energies Ψ_0. The most striking feature in Fig. 3 is that the Helmholtz energy of bcc phase decreases very rapidly as increasing the temperature, which cannot be expected from its initial slope (harmonic approximation) near the absolute zero temperature. This rapid decrease in the Helmholtz energy with temperature results from the anharmonicity of thermal lattice vibrations. Here, it should be noted that the anharmonicity effects of thermal lattice vibrations are more pronounced for the bcc phase with loser close packing structure (smaller lattice coordination numbers) and also for hcp structure with lower crystal symmetry compared to those of the closed packed fcc (cubic) structure, as can be seen in Fig. 3 by three free energy lines.

In order to see more clearly the contributions of vibrational entropy to the hcp→bcc transition, we also plot the differences in the vibrational free energies $\Delta\Psi_{vib}$ $(=\Psi_{vib}^{bcc} - \Psi_{vib}^{hcp}$, as defined in Ref. 12) between hcp and bcc phases as a function of temperature in Fig. 4. The solid curve in Fig. 4 shows the difference in the vibration free energy $\Delta\Psi_{vib}$ by the present SMM including the anharmonicity of thermal lattice vibrations, while the dashed one by Moroni *et al.*[12] in the quasiharmonic approximation. We also show in Fig. 4, by dot-dashed curve, the $\Delta\Psi_{vib}$ calculated in the harmonic approximation of the present method, without including the anharmonic contributions. It is noted that the harmonic approximation of the present SMM and quasiharmonic theory by Moroni *et al.*[12] give the positive $\Delta\Psi_{vib}$, which indicates that hcp phase becomes more stable than bcc phase upon increasing the temperature. Therefore, it has been claimed by Moroni *et al.*[12] that the electronic entropy plays an important role in the hcp→bcc phase transition of Ti crystal, and $T_c \approx 2050$ K has been calculated by them including the thermal electronic contributions. Here, it is remarkable that drastic changes occur in the $\Delta\Psi_{vib}$ behavior of Ti crystal, when one takes into account the anharmonicity effects of thermal lattice vibrations; the $\Delta\Psi_{vib}$ value becomes negative around T

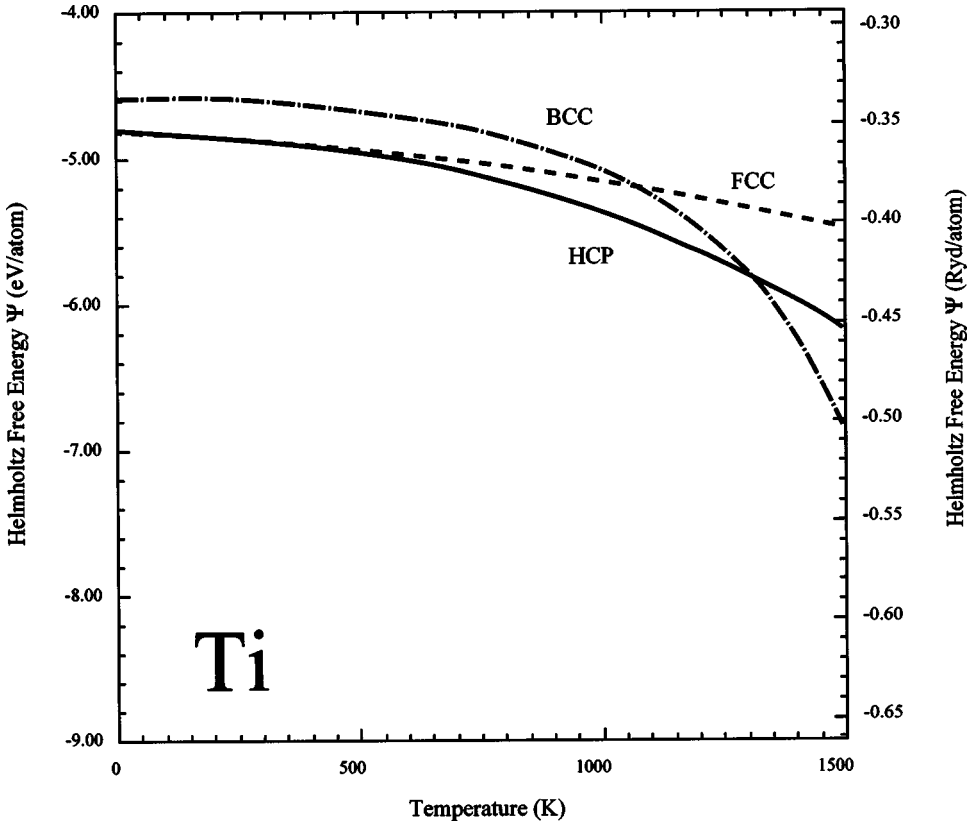

FIG. 3. Temperature dependences of Helmholtz free energies of Ti crystal for bcc, fcc, and hcp phases.

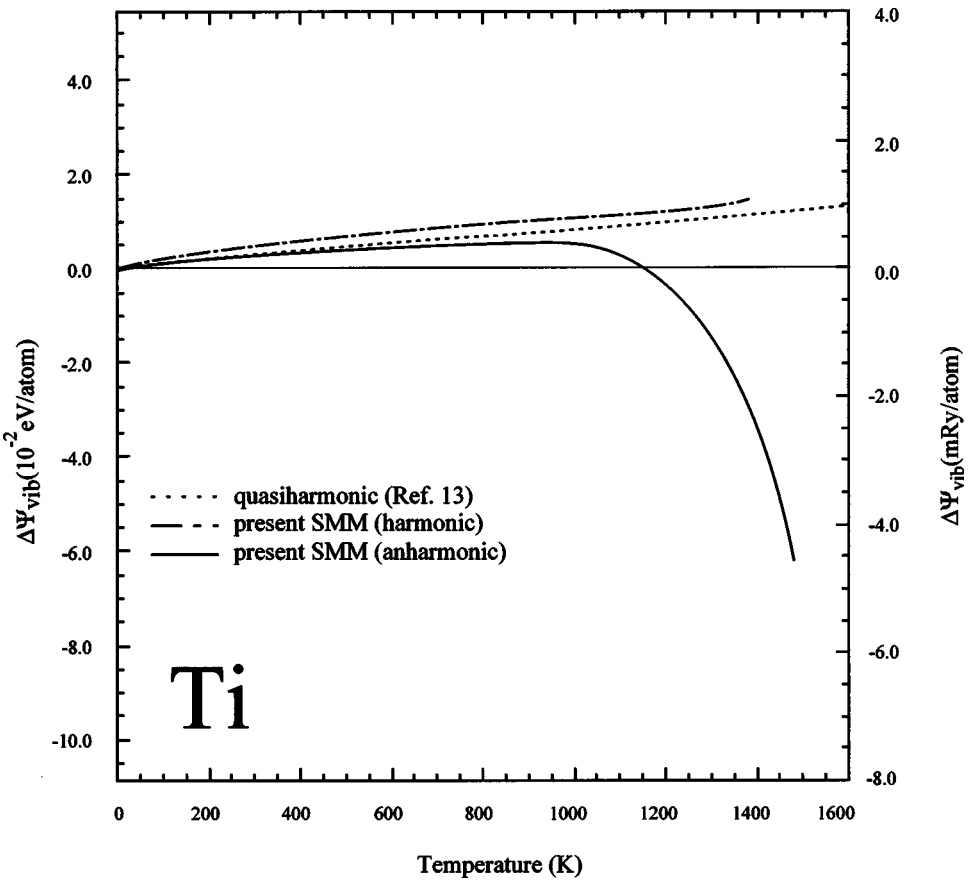

FIG. 4. The differences of the vibrational free energies $\Delta\Psi_{vib}$ between the bcc and hcp phases in the Ti crystals, by the present SMM and quasiharmonic approximations by Moroni *et al.* (Ref. 12).

$\approx$1150 K from positive value and bcc phase is stabilized strongly for higher temperatures in contrast to the harmonic $\Delta\Psi_{vib}$ (always positive) calculations.

The contribution of electronic entropy on the hcp-bcc transition is estimated from the standard entropy formula and electronic densities of states.[25] The thermal electronic entropy contribution obtained by the present FP-LMTO method is very close to that of Craievich *et al.*,[14] but it decreases the transition temperature T_c of Ti crystal only by $\sim$10 K in the present calculations. The calculated critical temperature T_c of hcp$\rightarrow$bcc transition including the electronic entropy contribution is shown in Table II, together with the transition temperatures of other calculations. In Table II, the hcp$\rightarrow$bcc transition temperature T_c of Ti crystal by the present SMM are referred to as cal-1 (1308 K) and cal-2 (1295 K), which are calculated without and with the thermal electronic contributions, respectively. The present T_c value of 1295 K is still higher than the experimental values of 1155–$\sim$1156 K, but we can expect that the T_c value of 1295 K can be decreased for more refined calculations, e.g., by including the higher order power moments than fourth order in the SMM and more direct use of the first-principles theory for the energetics. The transition temperatures T_c of hcp$\rightarrow$bcc transformation of Ti crystal have been calculated by a number of authors.[12,14,25] Moroni *et al.*[12] calculated the T_c of Ti crystal using the quasiharmonic approximation, and found that $T_c\approx$2050 K. On the other hand, Craievich *et al.*[14] calculated $T_c\approx$3350 K of Ti crystal, taking into account the thermal electronic contribution $\Psi_{band}(T)=E_{band}(T)-TS_{band}(T)$, without including the contributions of thermal lattice vibrations. The similar T_c value of 3300 K has also been obtained by Nishitani *et al.*[25] including only the thermal electronic contributions. The theoretical estimate of 3350 K by Craievich *et al.*[14] is significantly higher than that found (2050 K) by Moroni *et al.*[12] This difference, however, can be simply attributed to the hcp$\rightarrow$bcc ("internal") energy difference used in the T_c calculations (99 meV/atom versus 62 meV/atom, which can be understandable by simply scaling the temperatures by the hcp$\rightarrow$bcc energy differences). The discrepancy between the calculations most likely results from Moroni *et al.*'s use of the atomic-sphere approximation.[12]

TABLE II. Transition temperatures T_c of hcp$\rightarrow$bcc transition of Ti.

Present SMM Cal-1	Present SMM Cal-2	Moroni *et al.* (Ref. 12)	Craievich *et al.* (Ref. 14)	Exp.
1308	1295	2050	3350	1155

B. Zirconium crystal

Here, we also discuss the hcp$\rightarrow$bcc phase transformation occurring in zirconium in terms of the anharmonicity of thermal lattice vibrations. For comparison with the previous related theoretical calculations, we use the EAM potential of Zr derived recently by Pinsook and Ackland.[9] The calculated

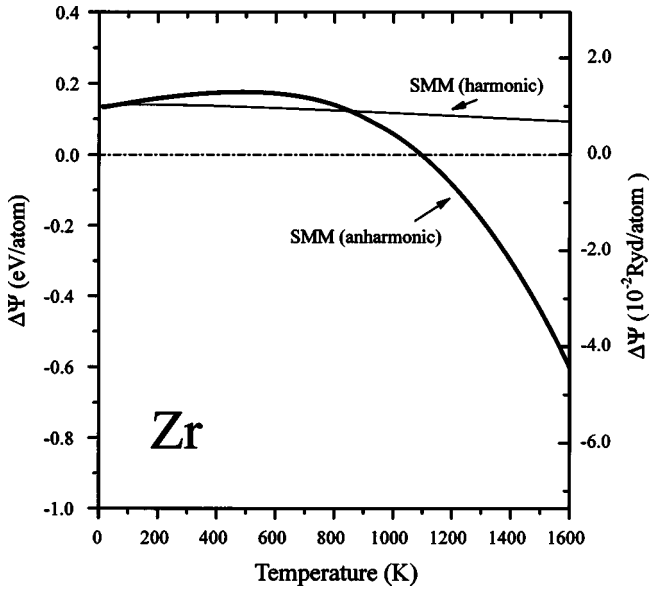

FIG. 5. Calculated values of the free energy difference $\Delta\Psi$ $(=\Psi_{bcc}-\Psi_{hcp})$ of Zr crystals as a function of temperature.

free energy differences $\Delta\Psi$ between bcc and hcp phases of Zr crystals by the present SMM scheme, both harmonic and anharmonic calculations, are presented in Fig. 5, by dot-dashed and solid lines, respectively. One can see in Fig. 5 that high temperature bcc phase of zirconium is stabilized within the harmonic approximation (even without the electronic entropy contributions), although the transition temperatures are estimated to be much higher than the experimental values. The anharmonic calculations give the reasonable transition temperature of zirconium. This tendency is consistent with the previous theoretical studies,[7–9,31] but qualitatively different from the hcp→bcc phase transition of titanium as discussed in the previous subsection. In general, the stabilities of high temperature bcc phase of Ti and Zr crystals can be attributed to the characteristic nonlinear dependence (decrease) of the anharmonicity parameters γ_1 and γ_2 with respect to the increase of bcc lattice spacings. The strong anharmonicity effects of thermal lattice vibrations in bcc Ti and Zr crystals have also been demonstrated in the recent study of neutron-scattering spectra by May *et al.*[32]

C. Mechanical instability

We now briefly comment on the phonon and/or mechanical instabilities of bcc phases of group IV-B elements. It is well known that at zero pressure and high temperature, all the group IV-B elements transform from the hcp to the bcc structure. This hcp to bcc phase transition occurs, in "phonon language," due to the anomalies of N-point phonon of the T_1 branch along the $[\xi\ \xi\ 0]$ direction. Accordingly, at zero temperature and zero pressure, the shear elastic moduli C' [defined by $C'=1/2(C_{11}-C_{12})$, where C_{11} and C_{12} are elastic constants] become negative and bcc crystal structures of group IV-B elements are mechanically unstable. The instability of bcc structure is observed experimentally at high temperature in all three metals.

As we have seen in the previous sections that the bcc structure is stabilized due to the thermal lattice vibration effects at high temperature. Therefore, one can expect that the high temperature bcc structure for these three elements shows anomalous properties. An example of this is the experimental observation that within the bcc phase these three metals become increasingly stiff with increasing temperature, a most unusual behavior.[10] Furthermore, it has been observed that IV-B elements (Zr and Hf) exhibit a crystal structure sequence hcp→ω→bcc, with increasing pressure.[10] In conjunction with the "mechanical instability" of the group IV-B elements, we have calculated the shear elastic constants C' of bcc Ti crystal as a function of the temperature as well as the function of atomic volumes (in other words, the hydrostatic pressure).

In Fig. 6(a), we present the calculated shear elastic constants C' of bcc Ti crystal at absolute zero temperature as a function of the relative atomic volumes (V/V_0), where V_0 denotes the atomic volume at zero pressure. The present results marked by symbols ○ are calculated by using the EAM potential of Eq. (14) fitted to the first-principles calculations, and they are compared with those of the previous theoretical calculations of Ahuja *et al.*,[10] by symbols △, obtained directly using the first-principles total energy calculations. One can see in Fig. 6(a) that the present calculations of the C' values are in good agreement with those by Ahuja *et al.*,[10] especially for the small volume relaxation region of (V/V_0) $\geqslant 0.85$. However, there are large discrepancies between the two results for smaller values of $(V/V_0)\leqslant 0.85$. The reason for the large discrepancy in the C' value between the two calculations is due to the fact that our EAM potential is composed of monotonous mathematical functions.

Also shown in Fig. 6(b) is the temperature dependence of shear elastic constants C' of bcc Ti crystal. In Fig. 6(b), the solid curve (cal-1) is calculated by fully taking into account the effects of thermal lattice vibrations, while the dashed curve (cal-2) without including the thermal lattice vibrations, but only taking into account the thermal lattice expansion of the bcc lattice. The most striking feature of our results are the dramatic changes of the shear elastic constant C', from negative to positive signs, upon increasing the temperature T. One can then expect that the stiffness of IV-B elements increases anomalously upon increasing the temperature, when C_{44} shows relatively the weak temperature dependence (this is the case of the present calculation).

IV. CONCLUSIONS

In conclusion, we have shown that bcc phase of Ti crystal becomes more stable than hcp phase for temperature region higher than the transition temperature T_c due to the anharmonicity effects of thermal lattice vibrations using the analytic calculations based on the statistical moment method. The predicted transition temperature $T_c\approx 1295$ K of Ti crystal is close to the experimental values (1155–~1156 K), and much lower than the previously reported theoretical value ~3350 K. It has been found that in the harmonic approximation and without including the thermal electronic contribution, hcp phase is always stable and hcp→bcc phase tran-

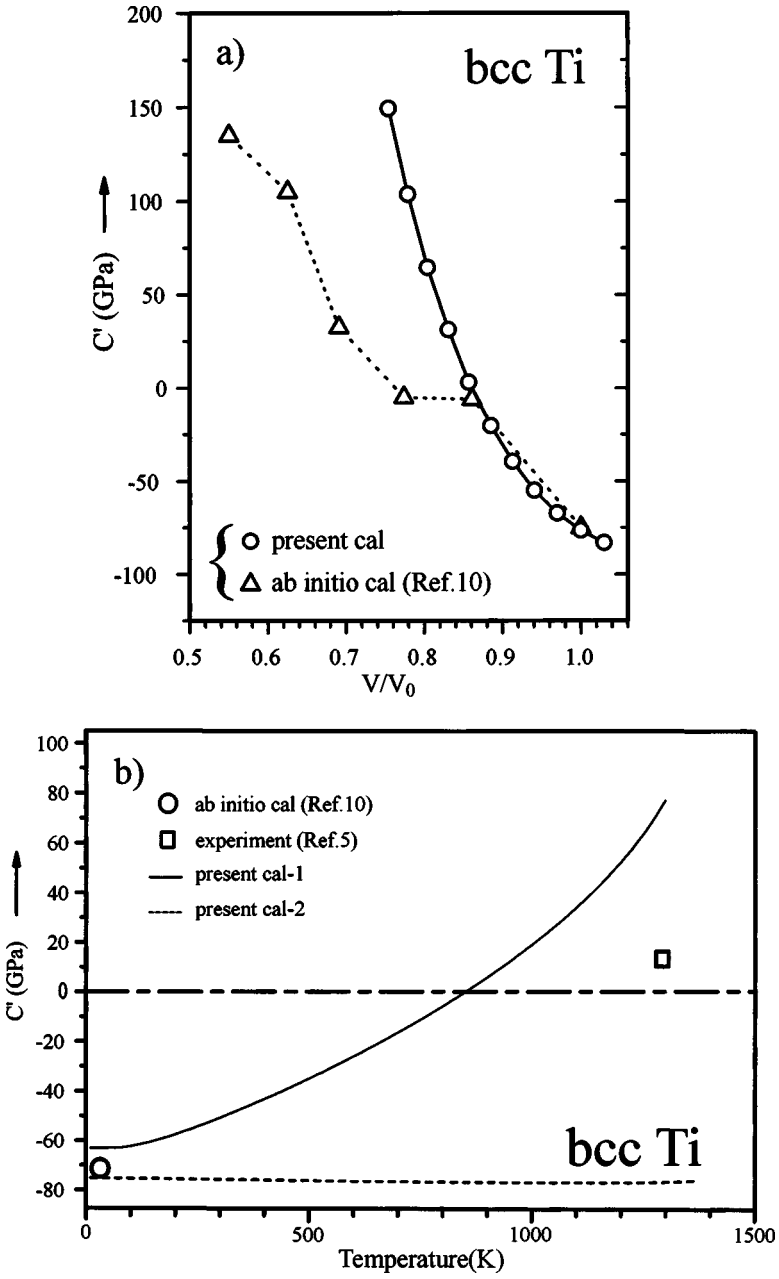

FIG. 6. The calculated shear elastic constants C' as a function of the relative atomic volume (a), and temperature dependence (b) of C' values in the bcc (β) Ti crystal.

sition never occurs in Ti crystal. The electronic entropy is an only minor contribution in determining the transition temperature T_c. For the hcp→bcc structural phase transformation of Zr, we have also obtained results consistent with the previous theoretical calculations.[7–9,31]

ACKNOWLEDGMENTS

The authors would like to thank Professor H. Takayama of Institute for Solid State Physics of the University of Tokyo for valuable discussions. The support of the supercomputing facility of Institute for Solid State Physics, the University of Tokyo is also acknowledged.

APPENDIX: SIMILARITY BETWEEN SMM AND "POTENTIAL SWITCH" MC METHOD

In this appendix, we will make a brief comment on the similarity between the present statistical moment method and the so-called "potential switch" Monte Carlo simulations,[22,33,34] originally developed by Frenkel and Ladd.[22] Following the potential switch MC (PSMC) method, for treating solid phase "harmonic solid" or "Einstein crystal" is taken as the reference system, for which the exact free energy expression is well known. For treating liquid phases, the ideal gas state is taken as a reference system. The basic idea is to construct a reversible path between the solid under consideration and an Einstein crystal with the same structure.

The Hamiltonian and the resulting free energy $\Psi(\lambda)$ of the system are, in a similar manner as in Eqs. (1) and (2), given by the following equations:

$$H(\lambda) = H_0 + \lambda V, \tag{A1}$$

$$\Psi(\lambda) = \Psi_0 + \int_0^{\lambda} \langle V \rangle_{\lambda'} d\lambda', \tag{A2}$$

where Ψ_0 denotes the free energy of the system with the unperturbed (harmonic Einstein) Hamiltonian H_0. Firstly, one can transform a given solid to an ideal Einstein crystal by adding a potential term of harmonic spring constants $\lambda V = \lambda \Sigma_{i=1}^{N} (r_i - r_i^0)^2$. For this case, we have the relation $\partial \Psi / \partial \lambda = \langle V \rangle_{\lambda}$. For treating the general case, the original reference state $\Psi(\lambda = 0)$ can be reached from the real solid by slowly switching on the spring constants while switching off the interatomic interactions:

$$\Psi(\lambda = 0) = \Psi(\lambda) - \int_0^{\lambda} \left\langle \frac{\partial H(\lambda')}{\partial \lambda'} \right\rangle d\lambda'. \tag{A3}$$

The free energy difference between the ideal Einstein crystal and the interacting Einstein crystal can be found numerically by performing a Monte Carlo simulation on the ideal Einstein crystal, in contrast to the analytic integrations I_1, I_2, and I_3 of the present SMM formalism.

This type of PSMC method is of great significance since it is capable of computing the absolute free energy of arbitrary solid phases. The simulation cells are accompanied by the so-called Einstein Crystal, as shown in Fig. 7, and MC simulation calculations can be done without any difficulties. One can then obtain the thermodynamic quantities of arbitrary solid phases, e.g., both hcp and bcc phases of Ti and Zr crystals.

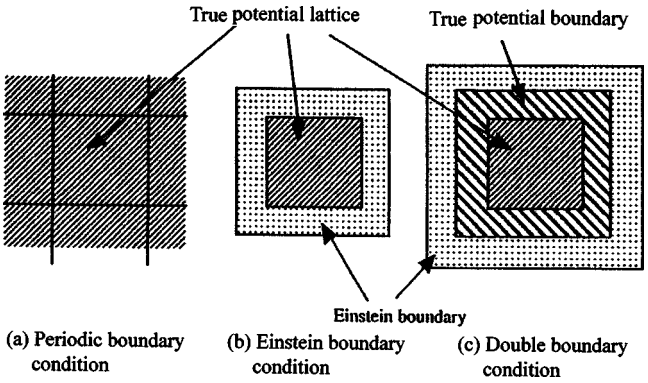

FIG. 7. Boundary conditions used in the PSMC simulations.

The efficiency of the original PSMC method has been improved by Watanabe and Reinhart[33] by introducing the appropriate time-dependent switching functions $\lambda(t)$. The intermediate Hamiltonian $H(\lambda)$ is now given by $H(\lambda) = \lambda H_1 + (1-\lambda) H_0$. The PSMC method has been further generalized by Sugino and Car,[34] by coupling with the first-principles density-functional theory. For treating the *ab initio* Hamiltonian $H_{ab\ initio}$, second reference system H_{model} is introduced, which is treated within the efficient empirical model potentials as

$$\Delta\Psi = \int_0^1 \langle H_{model} - H_{ref} \rangle_{\lambda'} d\lambda' + \int_0^1 \langle H_{ab\ initio} - H_{model} \rangle_{\lambda''} d\lambda''. \tag{A4}$$

The first application of this scheme was reported for the melting of silicon crystal.[34] It is also straightforward to generalize the present SMM to couple with the first-principles theory by simply evaluating the harmonic and anharmonic coupling parameters k and β, γ_1 and γ_2.

[1] C. Zener, Phys. Rev. **71**, 846 (1947).
[2] R. Hultgren, R. D. Desai, D. T. Hawkins, M. Gleiser, K. K. Kelly, and D. D. Wagman, *Selected Values of the Thermodynamic Properties of the Elements* (Am. Society for Metals, Metals Park, Ohio, 1973).
[3] Z. Nishiyama, *Martensitic Transformations* (Academic, New York, 1978).
[4] J. Friedel, J. Phys. (France) **35**, L59 (1974).
[5] W. Petry, A. Heiming, J. Trampenau, M. Alba, C. Herzig, H. R. Schober, and G. Vogl, Phys. Rev. B **43**, 10933 (1991); **43**, 10948 (1991); **43**, 10963 (1991).
[6] Y. Chen, C.-L. Fu, K.-M. Ho, and B. N. Harmon, Phys. Rev. B **31**, 6775 (1985).
[7] F. Willaime and C. Massobrio, Phys. Rev. B **43**, 11653 (1991).
[8] E. Salomons, Phys. Rev. B **43**, 6167 (1991).
[9] U. Pinsook and G. J. Ackland, Phys. Rev. B **59**, 13642 (1999); **58**, 11252 (1998); U. Pinsook, *ibid.* **66**, 024109 (2002).
[10] R. Ahuja, J. M. Wills, B. Johansson, and O. Eriksson, Phys. Rev. B **48**, 16269 (1993).
[11] G. Jomard, L. Maguad, and A. Pasturel, Philos. Mag. B **77**, 67 (1998).
[12] E. G. Moroni, G. Grimvall, and T. Jarlborg, Phys. Rev. Lett. **76**, 2758 (1996).
[13] O. Eriksson, J. M. Wills, and D. Wallace, Phys. Rev. B **46**, 5221 (1992).
[14] P. J. Craievich, J. M. Sanchez, R. E. Watson, and M. Weinert, Phys. Rev. B **55**, 787 (1997).
[15] J. C. Boettger and D. C. Wallace, Phys. Rev. B **55**, 2840 (1997).
[16] T. Jarlborg, E. G. Moroni, and G. Grimvall, Phys. Rev. B **55**, 1288 (1997).
[17] Y. Wang, Phys. Rev. B **61**, R11863 (2000).
[18] D. P. Landau and K. Binder, *A Guide to Monte Carlo Simulations in Statistical Physics* (Cambridge University Press, New York, 2000).
[19] K. Persson, M. Ekman, and V. Ozoliņš, Phys. Rev. B **61**, 11221 (2000).
[20] Vu Van Hung and K. Masuda-Jindo, J. Phys. Soc. Jpn. **69**, 2067 (2000).
[21] K. Masuda-Jindo, V. V. Hung, and P. D. Tam, Phys. Rev. B **67**, 094301 (2003).

[22] D. Frenkel and A. J. C. Ladd, J. Chem. Phys. **81**, 3118 (1984).
[23] W. G. Burgers, Physica (Amsterdam) **1**, 561 (1934).
[24] A. T. Paxton, M. Methfessel, and H. M. Polotoglou, Phys. Rev. B **41**, 8127 (1990).
[25] S. R. Nishitani, H. Kawabe, and M. Aoki, Mater. Sci. Eng., A **312**, 77 (2001).
[26] J. Perdew and Y. Wang, Phys. Rev. B **45**, 13244 (1992).
[27] J. Harris, Phys. Rev. B **31**, 1770 (1985).
[28] W. M. C. Foulkes and R. Haydock, Phys. Rev. B **39**, 12520 (1989).
[29] R. J. Wasilewski, Trans. Metall. Soc. AIME **221**, 1231 (1961).
[30] R. R. Pawar and V. T. Deshpande, Acta Crystallogr., Sect. A: Cryst. Phys., Diffr., Theor. Gen. Crystallogr. **24**, 316 (1968).
[31] S. A. Ostanin and V. Yu. Trubitsin, Phys. Rev. B **57**, 13485 (1998).
[32] T. May, W. Müller, and D. Strauch, Phys. Rev. B **57**, 5758 (1998).
[33] M. Watanabe and W. P. Reinhart, Phys. Rev. Lett. **65**, 3301 (1990).
[34] O. Sugino and R. Car, Phys. Rev. Lett. **74**, 1823 (1995).